Quaternary Research 82 (2014) 441–449

Contents lists available at ScienceDirect

Quaternary Research

journal homepage: www.elsevier.com/locate/yqres

Timing of the Northern Prince Gustav Ice Stream retreat and the deglaciation of northern James Ross Island, Antarctic Peninsula during the last glacial–interglacial transition

Daniel Nývlt [a,b,*], Régis Braucher [c], Zbyněk Engel [d,e], Bedřich Mlčoch [e], ASTER Team [c,1]

[a] Department of Geography, Faculty of Science, Masaryk University, Kotlářská 2, 611 37 Brno, Czechia
[b] Czech Geological Survey, Brno branch, Leitnerova 22, 658 69 Brno, Czechia
[c] Aix-Marseille Université, CNRS-IRD-Collège de France, UM 34 CEREGE, Technopôle de l'Arbois, BP80, 13545 Aix-en-Provence, France
[d] Faculty of Science, Charles University in Prague, Albertov 6, 128 43 Praha, Czechia
[e] Czech Geological Survey, Klárov 3, 118 21 Praha, Czechia

ARTICLE INFO

Article history:
Received 13 September 2013
Available online 27 June 2014

Keywords:
Northern Prince Gustav Ice Stream
Antarctic Peninsula Ice Sheet
Be-10 exposure dating
Schmidt hammer testing
Pleistocene–Holocene transition
James Ross Island

ABSTRACT

The Northern Prince Gustav Ice Stream located in Prince Gustav Channel, drained the northeastern portion of the Antarctic Peninsula Ice Sheet during the last glacial maximum. Here we present a chronology of its retreat based on in situ produced cosmogenic ^{10}Be from erratic boulders at Cape Lachman, northern James Ross Island. Schmidt hammer testing was adopted to assess the weathering state of erratic boulders in order to better interpret excess cosmogenic ^{10}Be from cumulative periods of pre-exposure or earlier release from the glacier. The weighted mean exposure age of five boulders based on Schmidt hammer data is 12.9 ± 1.2 ka representing the beginning of the deglaciation of lower-lying areas (<60 m a.s.l.) of the northern James Ross Island, when Northern Prince Gustav Ice Stream split from the remaining James Ross Island ice cover. This age represents the minimum age of the transition from grounded ice stream to floating ice shelf in the middle continental shelf areas of the northern Prince Gustav Channel. The remaining ice cover located at higher elevations of northern James Ross Island retreated during the early Holocene due to gradual decay of terrestrial ice and increase of equilibrium line altitude. Schmidt hammer R-values are inversely correlated with ^{10}Be exposure ages and could be used as a proxy for exposure history of individual granite boulders in this region and favour the hypothesis of earlier release of boulders with excessive ^{10}Be concentrations from glacier directly at this site. These data provide evidences for an earlier deglaciation of northern James Ross Island when compared with other recently presented cosmogenic nuclide based deglaciation chronologies, but this timing coincides with rapid increase of atmospheric temperature in this marginal part of Antarctica.

Introduction

The Antarctic Ice Sheet extended to the continental shelf edge in many locations during Quaternary glacial stages (Bentley, 1999; Davies et al., 2012) and commenced its most recent retreat during the last glacial–interglacial transition, i.e. between 15 and 8 ka (Anderson et al., 2002; Mackintosh et al., 2011). The retreat appears asynchronous around the whole Antarctic coastline; however, there is currently insufficient field data to bring a detailed chronology and extent of the last deglaciation of the Antarctic margins. Numerous ice streams drained the Antarctic Peninsula Ice Sheet during glacial times flowing down to the continental shelf edge (Johnson et al., 2011; Davies et al., 2012). Northern Prince Gustav Ice Stream (NPGIS) located in Prince Gustav Channel along the northeastern coast of the Antarctic Peninsula (AP) drained part of the Antarctic Peninsula Ice Sheet through the present Prince Gustav Channel to the east as evidenced by the sea floor bathymetry (Camerlenghi et al., 2001). Prince Gustav Channel is a pronounced over-deepened glacial trough between the AP and James Ross Island (JRI) up to 1000 m and 1200 m deep in its northern and southern part, respectively (Figs. 1A, B, Camerlenghi et al., 2001; Evans et al., 2005). The northern Prince Gustav Channel originated before the Late Miocene and experienced multiple advances of grounded glaciers during the Neogene and Quaternary (Nývlt et al., 2011).

The northern Prince Gustav Channel has not been covered by an ice shelf since the late 19th century AD, while the southern part was covered by the Prince Gustav Ice Shelf until its collapse in 1995 (Cooper, 1997; Cook and Vaughan, 2010). Pudsey and Evans (2001) demonstrated such collapses of the Prince Gustav Ice Shelf during the Holocene based on AMS radiocarbon data. The transition of the

* Corresponding author at: Department of Geography, Faculty of Science, Masaryk University, Kotlářská 2, 611 37 Brno, Czechia. Fax: +420 549 491 487.
E-mail address: daniel.nyvlt@seznam.cz (D. Nývlt).
[1] ASTER Team: Maurice Arnold, Georges Aumaître, Didier Bourlès, Karim Keddadouche.

http://dx.doi.org/10.1016/j.yqres.2014.05.003
0033-5894/

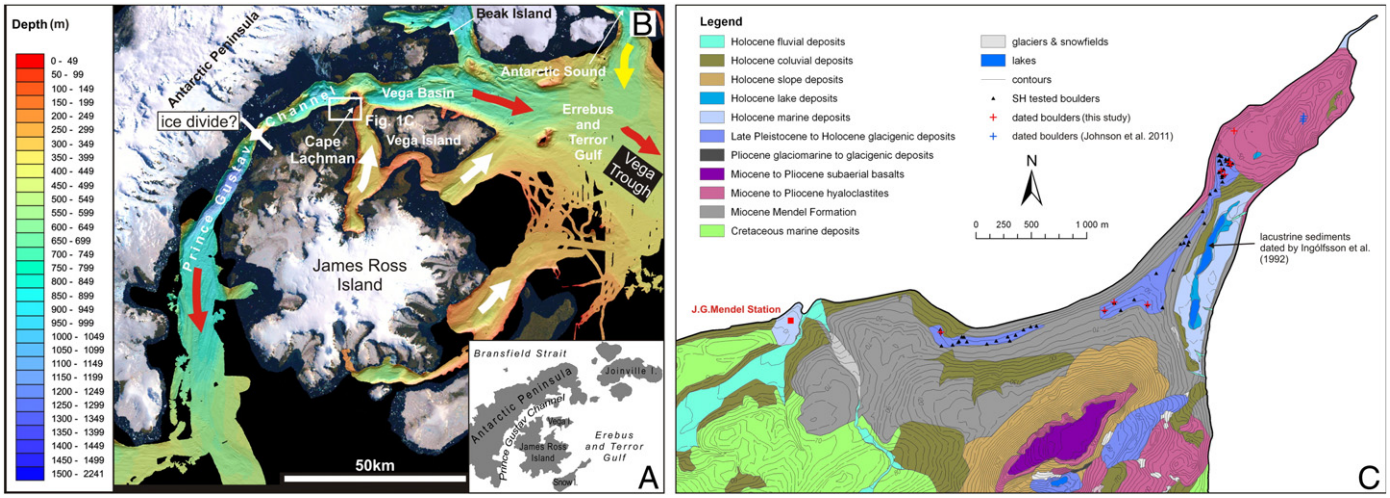

Figure 1. Location of glacigenic accumulation at the neck of the Cape Lachman showing sample site. A) The location of the James Ross Island at the eastern coast of the northern Antarctic Peninsula. B) Bathymetric map of the inner to middle continental shelf off the eastern coast of the Antarctic Peninsula, the relief is from the Landsat Image Mosaic of Antarctica (adopted from Johnson et al., 2011) with the study area. White arrows – former ice flow directions of JRI Ice Cap, red arrows – former ice flow directions of the Northern and Southern Prince Gustav Ice Streams separated by an ice divide, yellow arrow – ice flow direction of the Antarctic Sound Ice Stream. Important sites mentioned in text are also indicated. C) Geological sketch map of the northernmost part of the Ulu Peninsula, JRI. The extent of dated glacigenic accumulation is marked in blue, Schmidt hammered boulders are shown by black triangles and dated boulders by red crosses and those dated by Johnson et al. (2011) by blue crosses. Location of lacustrine sediments dated by Ingólfsson et al. (1992) is shown by an arrow. Topography based on the topographic map at the 1: 25 000 scale (Czech Geological Survey, 2009), geology based on own geological mapping, partly adopted from Nývlt et al. (2011).

southern Prince Gustav Channel from a grounded glacier to a floating ice shelf was completed by the end of the Pleistocene (cf. Pudsey and Evans, 2001; Evans et al., 2005; Johnson et al., 2011). The deglaciation of the northern part of JRI occurred as late as 10.7 cal ka BP (recalibrated age of 9.5 ^{14}C ka BP given by Ingólfsson et al. (1992)) based on the dating of aquatic moss from the Cape Lachman, northern JRI. Similarly, Roberts et al. (2011) and Sterken et al. (2012) presented a minimum radiocarbon age of 10.6 cal ka BP for the deglaciation of Beak Island on the opposite side of Prince Gustav Channel. The age constraints for these two sites are from the similar altitudes (10–15 m) and most likely represent the same deglaciation event around the Prince Gustav Channel (cf. Czech Geological Survey, 2009; Roberts et al., 2011).

Besides lacustrine sediments a well-preserved glacigenic accumulation with abundant erratic boulders originating from the AP was mapped at the neck of Cape Lachman, northern JRI (Fig. 1C; Nývlt et al., 2011). The deposition of this accumulation occurred during the last advance of the NPGIS; thus we were able to establish a terrestrial deglaciation chronology using in situ produced cosmogenic ^{10}Be in surface quartz mineral of selected boulders. Johnson et al. (2011) recently presented a deglaciation age of 8–9 ka for NPGIS using a minimum age model of ^{10}Be exposure ages of erratic boulders from ~110 m a.s.l. at Cape Lachman (Fig. 1C). However, the minimum deglaciation age given by Johnson et al. (2011) is younger than the radiocarbon ages of 10.6 to 13.9 cal ka BP obtained for postglacial organic material from this area (cf. Ingólfsson et al., 1992; Evans et al., 2005; Roberts et al., 2011).

In order to solve the discrepancy between radiocarbon and in situ produced ^{10}Be deglaciation chronologies of the low-lying areas of northern JRI and the deglaciation history of NPGIS in the middle to inner continental shelf (Fig. 1B), we present in situ produced ^{10}Be ages and Schmidt hammer (SH) rebound values of granite erratic boulders deposited during the retreat of the NPGIS. We believe that a combination of both methods, supported by appropriate statistical procedures, will improve the reliability in estimating the last deglaciation chronologies especially in flat low-lying regions at the Antarctic margin. However, this approach does not contradict deglaciation ages based on the more common mode of selecting the minimum exposure age samples for a given elevation as described in many Antarctic studies (e.g., Stone et al., 2003; Mackintosh et al., 2007; Storey et al., 2010; Johnson et al., 2011). This approach might help to reduce constraints that limit the interpretation of exposure data that may arise from i) the inheritance of cosmogenic ^{10}Be in boulders from previous exposure/s (e.g., Briner et al., 2003; Phillips et al., 2006); ii) initial burial of boulders, i.e. later exhumation from sediment due to the degradation of glacigenic accumulation by periglacial and/or aeolian processes (e.g., Putkonen and Swanson, 2003; Applegate et al., 2012).

Material and methods

Study site

The northern part of JRI is one of the largest deglaciated areas in Antarctica with only small glaciers remaining in the present landscape (Engel et al., 2012). Numerous isolated erratic boulders are scattered over the Cretaceous sedimentary and volcanic bedrock of the deglaciated terrain (Davies et al., 2013). A unique landform from the deglaciation phase of the northern part of the Ulu Peninsula, JRI is an accumulation of coastal erratic-rich drift at the neck of Cape Lachman (Fig. 1C; Davies et al., 2013) ranging in elevation from 25 to 60 m (mostly around 40 m a.s.l.). It is composed of up to 3 m large erratic boulders of granitoids from AP batholith (Leat et al., 1995) and metamorphic rocks from Trinity Peninsula Group (Barbeau et al., 2010) lying in an erratic-rich sandy to pebbly matrix. This sediment was deposited along the coast of JRI by advancing NPGIS over the lower saddle between Cape Lachman and Berry Hill during its last advance (Davies et al., 2013). Boulder surfaces are variably weathered and some of them are likely to have experienced longer or complex exposure and superficial weathering than others. Surface striations on some boulders are proof of limited erosion of boulder surfaces since they were released from the glacier for the last time. The accumulation overlies the Mendel Formation, a Late Miocene (5.9–5.4 Ma) glacial to marine sedimentary sequence within the James Ross Island Volcanic Group (Nývlt et al., 2011), which contains a similar suite of AP-derived erratic boulders up to at least 1 m large.

Schmidt hammer testing

Visual examination of boulder surfaces does not help to estimate their exposure/weathering history; therefore, we applied SH rock hardness measurements. Readings were made using N-type SH for 53 erratic granite boulders at the neck of Cape Lachman. We paid attention to

measure and sample only large boulders (>1 m in b-axis, Fig. 2) of medium-grained weakly porphyritic biotite granite of the Antarctic Peninsula Batholith originated probably from the Mt. Reece area (Žák et al., 2012), which were located at the flat surface, and for which periglacial ploughing is negligible. We applied the most accepted method among the different techniques of SH rebound measurements (e.g., Hubbard and Glasser, 2005). For each boulder, 25 hammer impacts were taken in accordance with the operating instructions recommended by Day and Goudie (1977). SH records were then processed following the guidelines presented by Moon (1984). Five values with the greatest deviation (outliers) were excluded from the original dataset and a new mean rebound value (R-value) was calculated from the remaining 20 values and taken as representative for that surface. To compare different R-values of individual boulders, the method proposed by Ward and Wilson (1978) was applied. This method is based on Chi-square analysis. To obtain the most adequate number of samples (n), a 0.05 critical value for a Chi-square with n-1 degrees of freedom is calculated from the distribution of all R-values and compared with the theoretical value given by Chi-square table. If the calculated value is lower than the theoretical one, then all samples are used to calculate a weighted mean R-value; otherwise outliers are rejected until the distribution passes the test and the weighted mean R-value for boulders is calculated with the remaining samples. All boulders with high R-values included in the final weighted mean R-value are considered as less weathered (and of similar exposure history) than those with lower R-values, which are found to be outliers with a more complex exposure/weathering history.

Cosmic ray exposure dating

To reduce the probability of post-depositional processes influencing the amount of in situ produced cosmogenic nuclides at the surface of the boulders we sampled only large granite boulders located on a flat surface. Samples for ^{10}Be exposure dating were collected from the upper surface (upper 3 cm) of each boulder. All samples were crushed and sieved prior to initiating chemical procedures. The extraction method for ^{10}Be consists of isolation and purification of quartz and elimination of atmospheric ^{10}Be. About 100 mg of a 3060 ppm ^{9}Be solution was weighted and added to the purified quartz, during dissolution with HF. Beryllium was extracted by controlled elution from successive anion and cation resin extraction (DOWEX 1X8 then 50WX8) columns. The final beryllium hydroxide precipitate was dried and heated at 800°C to obtain BeO and finally mixed with niobium powder prior to AMS measurements at the ASTER AMS Facility at CEREGE in Aix-en-Provence.

The ^{10}Be concentrations were calibrated directly against the National Institute of Standards and Technology standard reference material SRM-4325 by using an assigned value of $(2.79 \pm 0.03)\ 10^{-11}$. ^{10}Be exposure ages were based on a ^{10}Be half-life of $(1.387 \pm 0.012)\ 10^{6}$ years (Chmeleff et al., 2010; Korschinek et al., 2010). A modern ^{10}Be spallation production rate at sea-level and high-latitude of 4.49 ± 0.41 atoms/g/yr was used. Muons production follows the method of Braucher et al. (2011), where spallation production for slow muons and fast muons represents (0.043 ± 0.023) and

Figure 2. Individual dated boulders with apparent exposure ages indicated (B–I). General view of the glacigenic accumulation at the Cape Lachman neck with strongly weathered boulder in the forefield in (A). Note: the arrow in (C) indicates the location of the boulders at Cape Lachman dated by Johnson et al. (2011). Rock varnish on boulder (E) and (F). Visually more weathered boulder in (I).

(0.030 ± 0.012) at/gSiO_2/yr, respectively. The sea-level and high-latitude spallation production rate was then scaled for individual sample altitudes and latitudes using Stone (2000) polynomial while muon contributions were only scaled for altitude using Antarctic atmospheric pressure. Considering that partial shielding of the cosmic flux is negligible, a topographic shielding factor of 1 is used for production rate calculations. In order to determine ^{10}Be exposure ages from the ^{10}Be concentrations measured in the quartz fractions we used the equation of Braucher et al. (2011). Age uncertainties include 1-sigma error on counting statistics and instrumental error derived from multiple standard measurements. 1-sigma standard deviation of instrumental error is <0.5% based on multiple measurements of SRM-4325 standard during the considered run. Additionally, blank correction and an external AMS uncertainty of 0.5% (Arnold et al., 2010) integrates all effects contributing to ASTER's variability, including uncertainties from the current integrator, detector non-linearity with counting rates, terminal voltage stability and others. However, it is important to recall that ~9% uncertainty associated to the production rate has to be added to the analytical ones when comparison with other chronologies is performed. All ages have been calculated with a constant production rate implying that no correction was made for geomagnetic field variations, which are negligible in Antarctic latitude.

In order to investigate if the measured SH value can differentiate the ^{10}Be exposure age between less weathered and more weathered boulders (i.e., to find outliers) we sampled five fresh boulders (i.e., those with high R-values within the final population) and four weathered boulders (i.e., those for which the R-values are lower and are considered to be outliers) for ^{10}Be exposure dating. Similar to the statistical analysis of SH rebound data we applied the same Chi-square test (see above; Ward and Wilson, 1978) for the selection of our samples used for a calculation of weighted mean exposure age present here (Table 1). We have also recalculated ^{10}Be exposure ages from Cape Lachman area given by Johnson et al. (2011) using our age model (see Table 2 for the list of ^{10}Be exposure ages).

Calibration of radiocarbon dates

All previously published radiocarbon ages discussed here were recalibrated to allow comparison with ^{10}Be exposure ages. For marine radiocarbon ages the MARINE09 dataset of Reimer et al. (2009) was applied. A marine radiocarbon reservoir of 1280 ± 50 years based on modern bones at Hope Bay, northeastern AP (Björck et al., 1991) from the beginning of the 20th century was applied for the marine samples (except those of Pudsey and Evans, 2001; Evans et al., 2005 and Pudsey et al., 2006, for which a core-top correction of 6000 years was applied). Radiocarbon ages originating from freshwater samples were calibrated by using the SHCal04 dataset of McCormac et al. (2004). See Johnson et al. (2011) and the supplementary material therein for further details concerning calibration used to specific samples.

Results and interpretations

Schmidt hammer testing results

The mean SH R-values obtained for 53 erratic granite boulders range between 27.4 and 65.2 (Fig. 3; Supplementary material). We calculated a weighted mean R-value of 60.7 from the measurements (n = 35) that passed the Chi-square test. The upper limit of R-value for medium-grained granites, which we tested here, mostly ranges between 50 and 70 (cf. Goudie, 2006; Černá and Engel, 2011), which corresponds to our results. Therefore we hypothesize that the 35 boulders used to estimate the mean R-value are considered as fresh, sometimes with striated surfaces. We interpret these samples as the youngest population of the glacially transported material with exposure ages that would correspond to the most recent deglaciation. Using this approach we reduced the probability of sampling boulders for ^{10}Be exposure dating with

Table 1
^{10}Be concentrations. All ^{10}Be concentrations are normalized to ^{10}Be/^{9}Be SRM 4325 NIST standard with an assigned value of $(2.79 \pm 0.03)\cdot 10^{-11}$. Rock density is 2.65 g·cm^3. The third of the boulder dimensions is the boulder height above the present surface. Denudation is considered as negligible. Analytic uncertainties reflect 1 sigma analytical error. Total uncertainties reflect analytical uncertainties plus 9% of uncertainty on production rate. Samples LAC-02 till LAC-05 are originally published in Johnson et al. (2011).

Sample	Latitude (°S)	Longitude (°W)	Altitude (m)	Boulder dimensions (l × w × h in m)	Sample thickness (cm)	Relief shielding	Pressure (mbar)	Stone scaling	Spallation production (at·g^{-1}·yr^{-1})	^{10}Be concentration (atoms·g^{-1})	Age (yr)	Analytic uncertainty (yr)	Total uncertainty (yr)
DN 05-001	63.78935	57.80371	38	1.5·1.1·0.8	3	1	986.32	1.269	5.57	60 735 ± 11 873	10 792	2110	2322
DN 07-005	63.80179	57.85603	39	3.0·2.2·1.2	3	1	986.19	1.270	5.58	89 711 ± 5067	15 943	901	1694
DN 07-077	63.79955	57.82425	52	3.1·2.0·1.5	3	1	984.56	1.288	5.65	71 551 ± 4222	12 533	740	1349
DN 07-078	63.79979	57.81816	47	2.9·2.1·1.1	3	1	985.02	1.281	5.62	75 273 ± 4044	13 258	712	1390
DN 07-079	63.78900	57.80431	37	2.1·1.8·0.8	3	1	986.33	1.268	5.56	71 510 ± 3639	12 726	648	1316
DN 07-080	63.78583	57.8019	46	1.6·1.2·1.0	3	1	985.32	1.280	5.62	105 657 ± 5948	18 652	1050	1980
DN 07-081	63.78857	57.80261	43	1.8·1.4·0.7	3	1	986.30	1.276	5.60	74 487 ± 3246	13 173	574	1317
DN 09-111	63.78833	57.80275	43	1.7·1.2·1.0	3	1	985.70	1.276	5.60	124 471 ± 19 379	22 062	3435	3967
DN 09-091	63.80022	57.82603	50	1.5·1.1·0.9	3	1	984.81	1.285	5.64	142 132 ± 24 423	25 024	4300	4854
LAC-02	63.7847	57.7891	110	n.a.	5	1	977.30	1.369	5.91	50 159 ± 2050	8397	343	830
LAC-03	63.7851	57.7893	106	n.a.	5	1	977.80	1.363	5.89	51 228 ± 2022	8612	340	846
LAC-04	63.7851	57.7893	106	n.a.	5	1	977.80	1.363	5.89	67 759 ± 2695	11 398	453	1122
LAC-05	63.7849	57.7892	109	n.a.	6	1	977.42	1.368	5.86	51 786 ± 2715	8750	459	911

Table 2
Mean R-values and mean apparent exposure ages, including recalculated apparent exposure ages of the data from Johnson et al. (2011). Outliers have been discarded using a chi-square test. Regarding the numbers of samples (n) per accumulation, the 0.05 critical value for a Chi-square with (n-1) degrees of freedom is calculated (Experimental value) and compared with the theoretical one given by chi-square table. If the calculated value is lower than the theoretical one, then all samples are used to calculate a mean exposure age; if not, outliers are rejected, until the distribution passes the test and the mean exposure age and weighted R-values are calculated with the remaining samples. Samples LAC-02 till LAC-05 are originally published in Johnson et al. (2011).

	Sample	Mean R-value/CRE age (years)	Theoretical 95% Chi-square	Experimental 95% Chi-square	Theoretical 95% Chi-square	Experimental 95% Chi-square	Weighted mean R-value/weighted mean age
R-values	DN 05-001	60.8 ± 2.7	15.51	170.68	9.49	1.75	59.73 ± 1.21
	DN 07-081	60.0 ± 2.0	(n = 9)		(n = 5)		
	DN 07-077	54.3 ± 4.8					
	DN 07-078	58.8 ± 2.8					
	DN 07-079	60.9 ± 2.8					
	DN 07-080	34.9 ± 5.1			Outliers		
	DN 07-005	41.5 ± 5.2					
	DN 09-111	27.4 ± 2.4					
	DN 09-091	36.8 ± 4.5					
	LAC-04	57.7 ± 4.3			11.07 (n = 6)	1.96	Passed
Exposure ages	DN 05-001	10 792 ± 2110	15.51	49.10	9.49	1.80	12897 ± 325 (Weighted analytical uncertainties)
	DN 07-081	13 173 ± 574	(n = 9)		(n = 5)		12 897 ± 1205 (Weighted analytical uncertainties + 9% of production rate uncertainty)
	DN 07-077	12 533 ± 740					
	DN 07-078	13 258 ± 712					
	DN 07-079	12 726 ± 648					
	DN 07-080	18 652 ± 1050			Outliers		
	DN 07-005	15 943 ± 901					
	DN 09-111	25 024 ± 4300					
	DN 09-091	22 062 ± 3435					
	LAC-02	8397 ± 343			Outlier		
	LAC-03	8612 ± 340			Outlier		
	LAC-04	11 398 ± 453			11.07 (n = 6)	9.00	Passed
	LAC-05	8750 ± 459			Outlier		

excessive inheritance or earlier release from glacier by applying a SH test and a combined statistical criteria between ^{10}Be and SH datasets as described above. In order to test this hypothesis we sampled five of these 35 boulders for ^{10}Be exposure dating of the last deglaciation event according to our model (Fig. 4). The remaining 18 boulders with R-values ≤54.0 probably experienced longer or multiple exposures to weathering prior to the last deglaciation and thus should contain some inherited ^{10}Be or were uncovered earlier from the glacier. This group of more weathered boulders can be split into more subgroups according to their R-values (Fig. 3). They most likely represent the degree of previous exposure. In order to test this aspect of our hypothesis and to reconstruct the weathering/exposure histories of more weathered boulders, we sampled four boulders from this subgroup for CRE dating

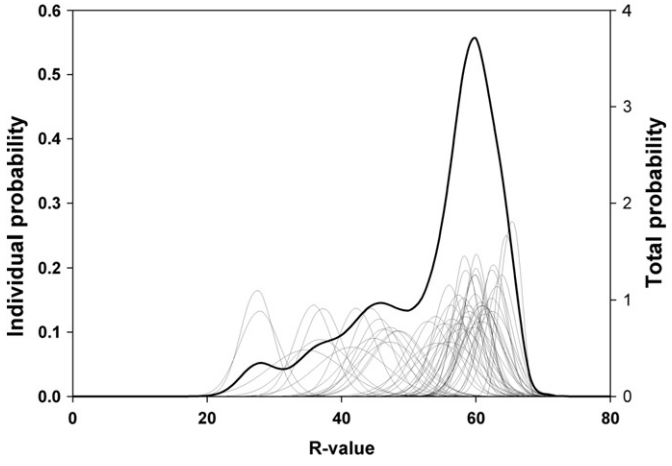

Figure 3. Normal kernel density estimate of all Schmidt hammer R-value data: the probabilities of individual boulders are marked by thin lines, the total probability by the thick line.

Cosmic ray exposure dating results

The apparent ^{10}Be exposure ages of the nine dated boulders range from 10.8 ± 2.1 ka to 25.0 ± 4.3 ka (Table 1). The combined analysis of R-values and apparent exposure ages show that fresh boulders with higher R-values have younger exposure ages and weathered boulders with lower R-values have older ages (Table 2, Fig. 4). We interpret the exposure age of the five fresh boulders to best represent with minimal inheritance or earlier release from glacier the timing of glacier retreat

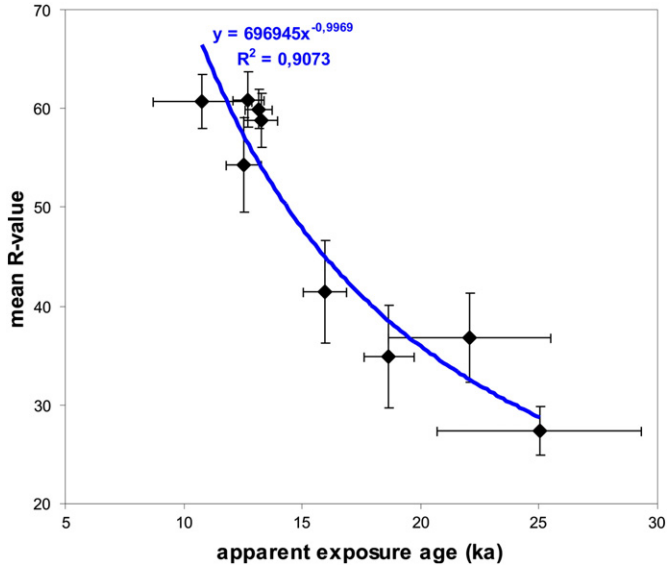

Figure 4. Covariant plot of ^{10}Be exposure age and mean R-value for nine boulders dated in this study. Best fitting power-law regression trend and equation plotted in blue.

from the neck of Cape Lachman. The other four apparent exposure ages (15.9 ± 0.9 ka to 25.0 ± 4.3 ka) represent a combination of the present exposure (since the last deglaciation) and previous exposures or earlier exposure during the NPGIS thinning (see Table 2 and Fig. 5).

The weighted mean age of the 5 fresh boulders is 12.9 ka with the analytical (1 sigma) uncertainty of 0.3 ka and the total uncertainty (including the uncertainty on production rate) of 1.2 ka. Individual ^{10}Be data for these five boulders, which passed the combined Chi-square test represents the same normally distributed population with a well-defined mean and standard deviation. This indicates that the boulders experienced similar exposure histories with minimal differences in possible pre-exposure or post-depositional changes. Hence, as an alternative solution to selecting the minimum exposure age of 10.8 ± 2.3 ka (DN05-001), we use the weighted mean age of 12.9 ± 1.2 ka (1 sigma uncertainty) as the most reliable deglaciation age for the glacigenic accumulation at the Cape Lachman neck. However, it could be shown that the minimum age and the mean age are statistically the same within the 1-sigma error.

Discussion

Weathering and exposure history of erratic boulders

The results presented here provide new method to assess the reliability of Antarctic exposure ages. The interpretation of ^{10}Be exposure data is site dependent, which is especially true for Antarctica. A commonly used approach is based on selecting the minimum exposure age for a given elevation for deglaciation as applied e.g. by Stone et al. (2003); Mackintosh et al. (2007); Storey et al. (2010); Johnson et al. (2011); White et al. (2011) or Balco et al. (2013). This method is particularly useful for cosmogenic age-versus-elevation profiles in Antarctic outlet glacier systems near ice sheet margins, where glacially derived debris is cumulative having been transported from multiple sites along the valley sides of the outlet glacier. Basically three main problems limit the use of boulders from glacigenic accumulations for direct dating (e.g., Fink et al., 2006; Applegate et al., 2012). They are 1) the inheritance of cosmogenic nuclide content from previous exposures prior to the last depositional event of the boulder, 2) longer exposure of the boulder due to earlier uncovering from glacier 3) post-depositional modification of the boulder upper surface position due to either its progressive later exhumation from sediment matrix or re-orientation due to moraine stabilisation.

The combined ^{10}Be exposure dating and SH testing provide additional information on the weathering and exposure histories of the studied boulders. R-values are markedly inversely correlated with ^{10}Be exposure ages (Fig. 4) and could thus be used as a proxy for exposure history of individual granite boulders in this region, which could be easily collected in the field. Apparent ^{10}Be exposure ages (15.9 ± 0.9 ka to 25.0 ± 4.3 ka) obtained for the four boulders with lower R-values do not represent the deglaciation age of Cape Lachman neck area. It is more likely a combination of the present (starting from the last deglaciation) and previous exposures. The effect of inheritance and thus previous exposure of boulders were reported earlier for the erratic material from JRI and Seymour Island (Johnson et al., 2011). We cannot tell much about the position of these four boulders during their previous exposure(s). However, a good inverse correlation between R-values and ^{10}Be exposure ages would favour the transport of some boulders in englacial or supraglacial position and their earlier release from glacier.

The ^{10}Be exposure ages of Johnson et al. (2011) were recalculated by using our age model (Table 1) to allow for comparison of ages from this study. It is evident that the age of 11.4 ± 0.5 ka (LAC-04; Johnson et al., 2011) falls within the cluster of our ^{10}Be data (Fig. 4) used to calculate the last deglaciation age and passed the combined Chi-square analysis of R-values and apparent exposure ages (Table 2). The other three ages from Johnson et al. (2011) sampled from ~50–80 m above our sampling altitude are younger than the ages from this study.

Deglaciation of northern James Ross Island

The results presented here provide new data on the initiation of NPGIS and northern JRI deglaciation. The last glacial NPGIS advance was responsible for a transport of large amounts of distal erratic AP debris either from their outcrops or from older sediments en route. A component of this debris was deposited along the margin of the ice stream and is now preserved at the neck of Cape Lachman. Based on the suite of five dated fresh boulders, we show that they were released from the ice at 12.9 ± 1.2 ka, which represents the last retreat of the NPGIS from this area.

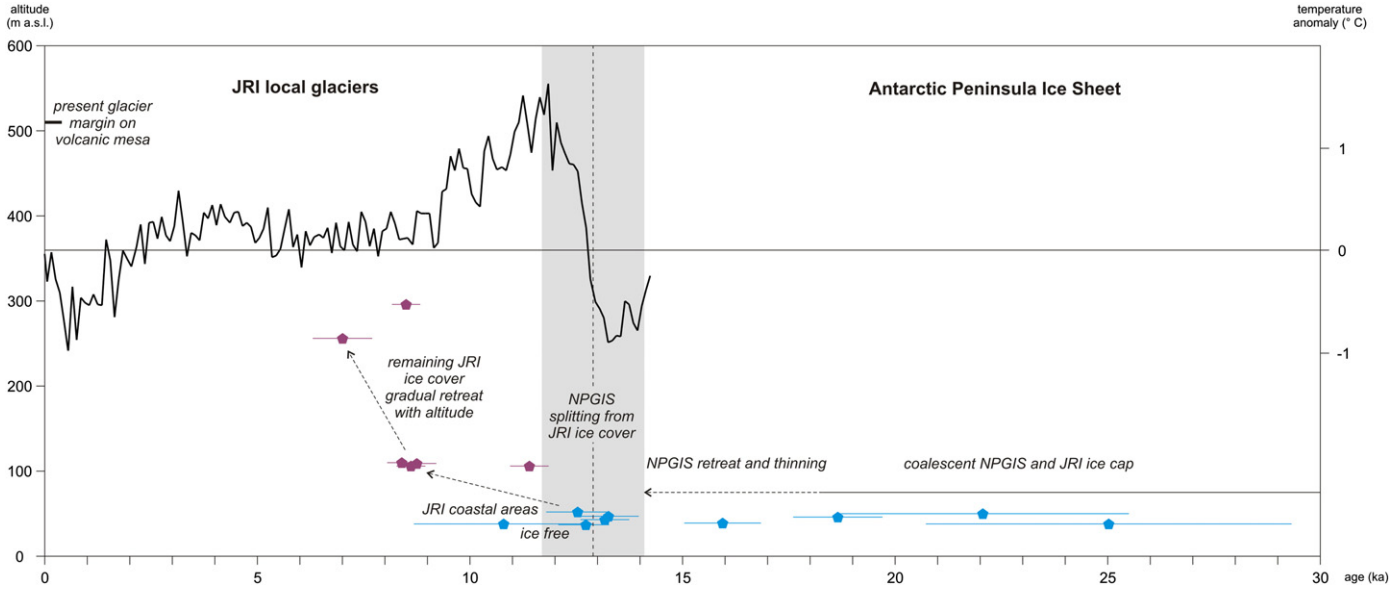

Figure 5. Interpreted late Pleistocene to early Holocene deglaciation chronology for the northern JRI based on ^{10}Be exposure ages from this study (blue) and recalculated ages for Cape Lachman elevation and Johnson Mesa are from Johnson et al., 2011 (violet) compared with recent glacier front altitude of the ice dome located on the southern Lachman Crags (thick black horizontal line). Grey column represents the range of 1-sigma uncertainty of the weighted mean deglaciation age for Cape Lachman neck area. Black graph shows 100-year average temperature anomalies record from the Mt. Haddington ice core (Mulvaney et al., 2012). Thin horizontal bar represents mean temperature of the period 1961–1990.

The deglaciation age obtained by ^{10}Be exposure dating of selected erratic boulders predates terrestrial organic dates reported for lacustrine sediments from the neck of Cape Lachman (10.7 cal ka BP; recalibrated age from Ingólfsson et al., 1992). An even older age of freshwater algae from southern Vega Island (11.8 ka; recalibrated age) was reported by Zale and Karlén (1989). The minimum deglaciation age of 10.6 ± 0.2 cal ka BP originates from Beak Island on the opposite side of Prince Gustav Channel, which represents the transition from glacial to marine environment (Roberts et al., 2011; Sterken et al., 2012; see Johnson et al., 2011 for a most comprehensive review of all marine and terrestrial radiocarbon data from this area and their recalibration).

Both Lachman Lakes with altitudes of 9 and 13 m (Czech Geological Survey, 2009; Nedbalová et al., 2013; see also Fig. 1C), from which the oldest dated freshwater material originates (Ingólfsson et al., 1992), lie immediately below the sampling sites for SH and ^{10}Be at the neck of Cape Lachman. The lakes lie below the local maximum Holocene marine limit of 15–20 m set by Ingólfsson et al. (1992). The studied accumulation lies between 25 and 60 m a.s.l. and most of the boulders lie in an altitude of 30–45 m. This clearly shows that marine processes could not affect the boulders since their release from the ice.

The highest (110 m a.s.l. based on Czech Geological Survey, 2009) fresh erratic boulders at Cape Lachman of Johnson et al. (2011) were exposed for at least 8.6 ± 0.9 ka (mean age model based on boulders LAC-02, LAC-04, LAC-05; see Table 1 for all recalculated ages) representing the mean age for total removal of all ice from the highest elevation site of the Cape Lachman promontory (Johnson et al., 2011). The oldest age of Johnson et al. (2011) recalculated by using our age model (11.4 ± 1.1 ka) lies within our mean age for the last deglaciation and the boulder is fresh according to the R-value (57.7 ± 4.3). We were unable to locate the other boulders sampled by Johnson et al. (2011), as they are rather small, as may be seen in Figure 2B in Johnson et al. (2011).

The initial deglaciation of the island was rather slow (Fig. 5). The coastal areas of JRI (this study) became ice-free by ~12.9 ka (Fig. 5). During this time the thinning and retreating NPGIS split from the remaining ice cover left on the surface of northern JRI and both glacier bodies evolved separately. Gradual increase of the local equilibrium line altitude implied retreat of terrestrial ice cover from lower elevations of JRI at the end of the Pleistocene and the beginning of the Holocene due to the temperature increase between 13 and 11 ka (Mulvaney et al., 2012). This warming led to the early Holocene temperature optimum (~11–12 ka), during which the coastal areas of JRI became ice-free. Subsequent local cooling between 11 and 9 ka (Mulvaney et al., 2012) decelerated glacier decay, therefore the areas around 100 m in altitude (Cape Lachman promontory) became ice-free around 8.6 ka (recalculated age of Johnson et al., 2011 using our age model; Fig. 5). The temperature has been rather stable and warm between 8.6 and 7.0 ka basing on the deuterium excess-based temperature anomalies from the JRI ice core (Mulvaney et al., 2012), which led to a more rapid deglaciation and volcanic mesas of Ulu Peninsula with altitudes about 300 m (Johnson Mesa) became ice-free at ~7.0 ka (recalculated age of Johnson et al., 2011 using our age model; Fig. 5). These data shows a different deglaciation model compared to ^{10}Be exposure data from a more proximal part of northern AP ice streams in the southern Prince Gustav Channel and former Larsen A ice shelf, where AP ice streams thinned gradually with time and then retreated, thus higher-lying elevation deglaciated first and low-lying areas became ice-free more recently (Balco et al., 2013). Local ice cover at JRI behaved individually after splitting from NPGIS and has been predominantly affected by altitude-dependent glacier front retreats.

Advances of local land-terminating valley glaciers have been reported at different scales for the mid-Holocene (Hjort et al., 1997) and late Holocene (or "Little Ice Age") times (Carrivick et al, 2012), when the local equilibrium line altitude was significantly lower than at present (Nývlt et al., 2010; Engel et al., 2012). We do not have enough data to reconstruct the deglaciation of northern Ulu Peninsula during the mid- and late Holocene period, especially for higher altitudes. The present front of a small ice dome on the Lachman Crags lies at ~510 m (Fig. 5; Czech Geological Survey, 2009). The generally low-lying landscape of northern Ulu Peninsula, JRI has thus remained ice-free for most of the Holocene due to the absence of higher-located accumulation areas for local glaciers. However, the remaining ice cover on higher-located (>600 m) volcanic mesas has probably persisted since at least the Pleistocene, as was demonstrated by Johnson et al. (2009) for Patalamon Mesa on the western coast of JRI.

Northern Prince Gustav Ice Stream deglaciation chronology

Scarce chronological evidence exists for the deglaciation history of the northeastern part of the AP shelf along the sector of Erebus and Terror Gulf and northern Prince Gustav Channel (see Fig. 1B). Deglaciation of the Weddell Sea outer shelf in this locality started around 18.3 cal ka BP (recalibrated age of Heroy and Anderson, 2007). The retreat from the outer shelf to inner shelf took place between 18.3 and 12.9 ka. We have not much evidence for the middle shelf (Erebus and Terror Gulf and Vega Basin; Fig. 1B) deglaciation history. The only exception is the attempt of a programmed-temperature pyrolysis/combustion method applied for radiocarbon dating of the sample from the KC-49 core drilled in the middle Erebus and Terror Gulf close to the Antarctic Sound (Rosenheim et al., 2008). The recalibrated age of their low temperature radiocarbon dating results gives the age of the uppermost parts of muddy diamictons deposited by a grounding glacier at 11.5 ± 0.2 cal ka BP. Despite the improvement of the method, the actual age of the sediment dated from KC-49, while better constrained, remains unknown (Rosenheim et al., 2008). It is very probable that the most important retreat from outer to middle shelf occurred during meltwater pulse 1A, i.e. ~14.5–14.0 ka (Weaver et al., 2003; Clark et al., 2009).

In spite of the subsequent climatic deterioration during the Antarctic Cold Reversal (~14.1–12.4 ka; Stenni et al., 2001) around Antarctica, individual ice streams of the northeastern part of AP continued to retreat as was shown for the Southern Prince Gustav Ice Stream by Evans et al. (2005) and Pudsey et al. (2006). This was caused by a pronounced local atmospheric warming starting at ~13.0 ka detected by deuterium excess-based temperature anomalies from the JRI ice core (Mulvaney et al., 2012). The change of the grounded glaciers to floating ice shelves and the grounding zone retreat has also been affected by the rising sea level connected with the continuing thawing of Northern Hemisphere ice sheets (e.g., Rinterknecht et al., 2006; Simms et al., 2007). The debuttressing effect from break-up of ice shelf edges accelerate retreat and affected coastal lower-lying land areas, which have ceased to be supplied by ice from ice streams and deglaciated rapidly, as is the case with the neck of Cape Lachman, northern JRI.

From the viewpoint of the NPGIS, the retreat of the glacier in the area of Prince Gustav Channel near Cape Lachman represents the transition from middle to inner shelf. The ^{10}Be deglaciation age reported here postdates the transition from grounded ice stream to floating ice shelf. Therefore, this transition from middle to inner shelf part of the northern Prince Gustav Channel took place prior to 12.9 ka. This is similar to the southern part of Prince Gustav Channel, where transition occurred between 13.9 and 10.5 cal ka BP (recalibrated ages of Pudsey and Evans, 2001; Pudsey et al., 2006 by Johnson et al., 2011), but more probably at the beginning of this interval. This is because the timing of deglaciation of NPGIS was influenced by the seafloor bathymetry (Johnson et al., 2011) and higher-lying land areas of JRI remained glaciated when the glacier in Prince Gustav Channel became a floating ice shelf. However, the main problem in comparing ^{10}Be exposure ages with radiocarbon ages in the surrounding of the James Ross Island archipelago is that the organic matter from bulk sediment is affected by reworked carbon from kerogen originating from Cretaceous sedimentary rocks (e.g., Brachfeld et al., 2003). Thus much more work is needed to improve

chronological constrains of the deglaciation history based on the radiocarbon dating of marine samples.

Early Holocene transition from grounded glacier to floating ice shelf is reported from the more distant Larsen A and B ice shelves along the eastern coast of the AP. The minimum transition age of 10.7 ± 0.5 ka was obtained by the palaeomagnetic intensity cross-dating of the marine sediments in the inner continental shelf of the Larsen A sector (Brachfeld et al., 2003). Slightly later transition was found for the inner continental shelf of the Larsen B Ice Shelf based on the radiocarbon dating of calcareous foraminifera (10.2 ± 0.1 cal ka BP; recalibrated age from Domack et al., 2005) from the base of the sub-ice shelf facies of the Larsen B Ice Shelf. The beginning of the deglaciation at 13.2 ka reported from the Palmer Deep at the western coast of the AP was interpreted as the onset of marine deposition following the grounded glacier retreat (Domack et al., 2001; Brachfeld et al., 2002). The deglaciation ages are slightly younger farther south along the western coast of AP. Deglaciation of inner shelf in Southern Bellingshausen Sea took place at 12.3 ka (Hillenbrand et al., 2010). The transition ages of individual grounded ice streams to floating ice shelves around the AP thus reflect a north-south trend on both sides of the AP. However, the western continental shelf of the AP deglaciated generally earlier than its eastern shelf.

Conclusions

Combination of SH testing and ^{10}Be exposure dating has been used to reconstruct deglaciation history of NPGIS and northern JRI during the last glacial–interglacial transition. The approach applied here reduces sources of potential errors (i.e., the inheritance of cosmogenic ^{10}Be, earlier release from glacier, or later exhumation from sediment) and can provide a reliable measure of timing of the last deglaciation. A weighted mean exposure age is preferred for our dataset, where statistical analysis confirms that ^{10}Be exposure ages are grouped in clusters. Furthermore, SH R-values are markedly inversely correlated with ^{10}Be exposure ages and could be used as a proxy for exposure history of erratic granite boulders in this region.

According to the new exposure ages provided by this study, the low-lying areas of the northern JRI became ice-free at around 12.9 ka. During that time the thinning NPGIS detached from the remaining ice cover of northern JRI and since then both glacier bodies behaved separately. The higher parts of the island deglaciated in the early Holocene due to the gradual altitude-dependent retreat of local glaciers. At the time of the deglaciation of low-lying areas, the grounded NPGIS changed to a floating ice shelf in the middle-inner continental shelf. The transition from grounded ice to floating ice shelves around the Antarctic Peninsula reflects a north-south and west-east trend; thus the northern Prince Gustav Channel was one of the first deglaciated trough valleys around the Antarctic Peninsula. The data from this study provide evidence for an earlier deglaciation of northern James Ross Island when compared with other recently presented cosmogenic nuclide-based deglaciation chronologies. Its timing coincides, however, with the rapid increase of atmospheric temperature in this marginal part of Antarctica.

Acknowledgments

This study was financially supported by R & D project VaV SP II 1a9/23/07 of the Ministry of the Environment of the Czech Republic and by the grant of the Czech Science Foundation 205/09/1876. The fieldwork at JRI was undertaken by DN, ZE and BM mostly during the austral summer seasons of 2005, 2007 and 2009, when we appreciate we could use the scientific infrastructure of the Czech Antarctic J.G. Mendel Station and the support of its crew. DN's final work on this paper has been supported by the project "Employment of Best Young Scientists for International Cooperation Empowerment" (CZ.1.07/2.3.00/30.0037) co-financed from European Social Fund and the state budget of the Czech Republic. We are grateful for the discussion of different topics to Neil Glasser and Joanne Johnson. We very much appreciate the reviews of Greg Balco and Lauren Simkins and especially the helpful suggestions of Associate Editor David Fink. The ^{10}Be measurements were performed on ASTER AMS national facility (CEREGE, Aix-en-Provence), which is supported by the INSU/CNRS, the French Ministry of Research and Higher Education, IRD and CEA.

Appendix A. Supplementary data

Supplementary data to this article can be found online at http://dx.doi.org/10.1016/j.yqres.2014.05.003.

References

Anderson, J.B., Shipp, S.S., Lowe, A.L., Wellner, J.S., Mosola, A.B., 2002. The Antarctic ice sheet during the last glacial maximum and its subsequent retreat history: a review. Quaternary Science Reviews 21, 49–70.

Applegate, P.J., Urban, N.M., Keller, K., Lowell, T.V., Laabs, B.J.C., Kelly, M.A., Alley, R.B., 2012. Improved moraine age interpretations through explicit matching of geomorphic process models to cosmogenic nuclide measurements from single landforms. Quaternary Research 77, 293–304.

Arnold, M., Merchel, S., Bourlès, D.L., Braucher, R., Benedetti, L., Finkel, R.C., Aumaître, G., Gottdang, A., Klein, M., 2010. The French accelerator mass spectrometry facility ASTER: improved performance and developments. Nuclear Instruments and Methods in Physics Research B 268, 1954–1959.

Balco, G., Schaefer, J.M., LARISSA group, 2013. Exposure-age record of Holocene ice sheet and ice shelf change in the northeast Antarctic Peninsula. Quaternary Science Reviews 59, 101–111.

Barbeau, D.L., Davis, J.T., Murray, K.E., Valencia, V., Gehrels, G.E., Zahid, K.M., Gombosi, D.J., 2010. Detrital-zircon geochronology of the metasedimentary rocks of north-western Graham Land. Antarctic Science 22, 65–78.

Bentley, M.J., 1999. Volume of Antarctic ice at the Last Glacial Maximum, and its impact on global sea level change. Quaternary Science Reviews 18, 1569–1595.

Björck, S., Hjort, C., Ingólfsson, Ó., Skog, G., 1991. Radiocarbon dates from the Antarctic Peninsula Region—Problems and potential. Quaternary Proceedings 1, 55–65.

Brachfeld, S.A., Banarjee, S.K., Guyodo, Y., Acton, G.D., 2002. A 13 200 year history of century to millennial-scale palaeoenvironmental change magnetically recorded in the Palmer Deep, western Antarctic Peninsula. Earth and Planetary Science Letters 194, 311–326.

Brachfeld, S., Domack, E., Kissel, C., Laj, C., Leventer, A., Ishman, S., Gilbert, R., Camerlenghi, A., Eglinton, L.B., 2003. Holocene history of the Larsen-A Ice Shelf constrained by geomagnetic paleointensity dating. Geology 31, 749–752.

Braucher, R., Merchel, S., Borgomano, J., Bourlès, D.L., 2011. Production of cosmogenic radionuclides at great depth: a multi element approach. Earth and Planetary Science Letters 309, 1–9.

Briner, J.P., Miller, G.H., Davis, P.T., Bierman, P.R., Caffee, M., 2003. Last Glacial Maximum ice sheet dynamics in Arctic Canada inferred from young erratics perched on ancient tors. Quaternary Science Reviews 22, 437–444.

Camerlenghi, A., Domack, E., Rebesco, M., Gilbert, R., Ishman, S., Leventer, A., Brachfeld, S., Drake, A., 2001. Glacial morphology and post-glacial contourites in northern Prince Gustav Channel (NW Weddell Sea, Antarctica). Marine Geophysical Research 22, 417–443.

Carrivick, J.L., Davies, B.J., Glasser, N.F., Nývlt, D., Hambrey, M.J., 2012. Late-Holocene changes in character and behaviour of land-terminating glaciers on James Ross Island, Antarctica. Journal of Glaciology 58 (212), 1176–1190.

Černá, B., Engel, Z., 2011. Surface and sub-surface Schmidt hammer rebound value variation for a granite outcrop. Earth Surface Processes and Landforms 36, 170–179.

Chmeleff, J., von Blanckenburg, F., Kossert, K., Jakob, D., 2010. The determination of the ^{10}Be half-life by multicollector ICP-MS and liquid scintillation counting. Nuclear Instruments and Methods in Physics Research B 268, 192–199.

Clark, P.U., Dyke, A.S., Shakun, J.D., Carlson, A.E., Clark, J., Wohlfarth, B., Mitrovica, J.X., Hostetler, S.W., McCabe, A.M., 2009. The Last Glacial Maximum. Science 325, 710–714.

Cook, A.J., Vaughan, D.G., 2010. Overview of areal changes of the ice shelves on the Antarctic Peninsula over the past 50 years. The Cryosphere 4, 77–98.

Cooper, A.P.R., 1997. Historical observations of Prince Gustav Ice Shelf. Polar Record 33, 285–294.

Czech Geological Survey, 2009. James Ross Island - Northern Part. Topographic map 1: 25 000. CGS, Praha.

Davies, B.J., Hambrey, M.J., Smellie, J.L., Carrivick, J.L., Glasser, N.F., 2012. Antarctic Peninsula Ice Sheet evolution during the Cenozoic Era. Quaternary Science Reviews 31, 30–66.

Davies, B.J., Glasser, N.F., Carrivick, J.L., Hambrey, M.J., Smellie, J.L., Nývlt, D., 2013. Landscape evolution and ice-sheet behaviour in a semi-arid polar environment: James Ross Island, NE Antarctic Peninsula. In: Hambrey, M.J., Barker, P.F., Barrett, P.J., Bownam, V., Davies, B., Smellie, J.L., Tranter, M. (Eds.), Antarctic Palaeoenvironments and Earth-Surface Processes. Geological Society of London, Special Publication, 381, pp. 353–395.

Day, M.J., Goudie, A.S., 1977. Field assessment of rock hardness using the Schmidt test hammer. British Geomorphology Research Group Technical Bulletin 18, 19–29.

Domack, E., Leventer, A., Dunbar, R., Taylor, F., Brachfeld, S., Sjunneskog, C., ODP Leg 178 Scientific Party, 2001. Chronology of the Palmer Deep site, Antarctic Peninsula:

a Holocene palaeoenvironmental reference for the circum-Antarctic. The Holocene 11, 1–9.
Domack, E., Duran, D., Leventer, A., Ishman, S., Doane, S., McCallum, S., Amblas, D., Ring, J., Gilbert, R., Prentice, M., 2005. Stability of the Larsen B ice shelf on the Antarctic Peninsula during the Holocene epoch. Nature 436, 681–685.
Engel, Z., Nývlt, D., Láska, K., 2012. Ice thickness, areal and volumetric changes of Davies Dome and Whisky Glacier (James Ross Island, Antarctic Peninsula) in 1979–2006. Journal of Glaciology 58 (211), 904–914.
Evans, J., Pudsey, C.J., ÓCofaigh, C., Morris, P., Domack, E., 2005. Late Quaternary glacial history, flow dynamics and sedimentation along the eastern margin of the Antarctic Peninsula Ice Sheet. Quaternary Science Reviews 24, 741–774.
Fink, D., McKelvey, B., Hambrey, M.J., Fabel, D., Brown, R., 2006. Pleistocene deglaciation chronology of the Amery Oasis and Radok Lake, northern Prince Charles Mountains, Antarctica. Earth and Planetary Science Letters 243, 229–243.
Goudie, A.S., 2006. The Schmidt Hammer in geomorphological research. Progress in Physical Geography 30, 703–718.
Heroy, D.C., Anderson, J.B., 2007. Radiocarbon constraints on Antarctic Peninsula Ice Sheet retreat following the Last Glacial Maximum (LGM). Quaternary Science Reviews 26, 3286–3297.
Hillenbrand, C.-D., Larter, R.D., Dowdeswell, J.A., Ehrmann, W., Ó Cofaigh, C., Benetti, S., Graham, A.G.C., Grobe, H., 2010. The sedimentary legacy of a palaeo-ice stream on the shelf of the southern Bellingshausen Sea: clues to West Antarctic glacial history during the Late Quaternary. Quaternary Science Reviews 29, 2741–2763.
Hjort, C., Ingólfsson, Ó., Möller, P., Lirio, J.M., 1997. Holocene glacial history and sea-level changes on James Ross Island, Antarctic Peninsula. Journal of Quaternary Science 12, 259–273.
Hubbard, B., Glasser, N., 2005. Field Techniques in Glaciology and Glacial Geomorphology. Wiley, Chichester, [400 pp.].
Ingólfsson, Ó., Hjort, C., Björck, S., Smith, R.I.L., 1992. Late Pleistocene and Holocene glacial history of James Ross Island, Antarctic Peninsula. Boreas 21, 209–222.
Johnson, J.S., Smellie, J.L., Nelson, A.E., Stuart, F.M., 2009. History of the Antarctic Peninsula Ice Sheet since the early Pliocene—Evidence from cosmogenic dating of Pliocene lavas on James Ross Island, Antarctica. Global and Planetary Change 69, 205–213.
Johnson, J.S., Bentley, M.J., Roberts, S.J., Binnie, S.A., Freeman, S.P.H.T., 2011. Holocene deglacial history of the northeast Antarctic Peninsula — A review and new chronological constraints. Quaternary Science Reviews 30, 3791–3802.
Korschinek, G., Bergmaier, A., Faestermann, T., Gerstmann, U.C., Knie, K., Rugel, G., Wallner, A., Dillmann, I., Dollinger, G., Lierse von Gostomski, C., Kossert, K., Maiti, M., Poutivtsev, M., Remmert, A., 2010. A new value for the half-life of ^{10}Be by heavy ion elastic recoil detection and liquid scintillation counting. Nuclear Instruments and Methods in Physics Research B 268, 187–191.
Leat, P.T., Scarrow, J.H., Millar, I.L., 1995. On the Antarctic Peninsula batholith. Geological Magazine 132, 399–412.
Mackintosh, A., White, D., Fink, D., Gore, D.B., Pickard, J., Fanning, P.C., 2007. Exposure ages from mountain dipsticks in Mac. Robertson Land, East Antarctica, indicate little change in ice-sheet thickness since the Last Glacial Maximum. Geology 35, 551–554.
Mackintosh, A., Golledge, N., Domack, E., Dunbar, R., Leventer, A., White, D., Pollard, D., DeConto, R., Fink, D., Zwartz, D., Gore, D., 2011. Retreat of the East Antarctic ice sheet during the last glacial termination. Nature Geoscience 4, 195–202.
McCormac, F.G., Hogg, A.G., Blackwell, P.G., Buck, C.E., Higham, T.F.G., Reimer, P.J., 2004. SHCal04 Southern Hemisphere Calibration, 0–11.0 cal kyr BP. Radiocarbon 46, 1087–1092.
Moon, B.P., 1984. Refinement of a technique for determining rock mass strength for geomorphological purposes. Earth Surface Processes and Landforms 9, 189–193.
Mulvaney, R., Abram, N.J., Hindmarsh, R.C.A., Arrowsmith, C., Fleet, L., Triest, J., Sime, L.C., Alemany, O., Foord, S., 2012. Recent Antarctic Peninsula warming relative to Holocene climate and ice-shelf history. Nature 489, 141–144.
Nedbalová, L., Nývlt, D., Kopáček, J., Šobr, M., Elster, J., 2013. Freshwater lakes of Ulu Peninsula, James Ross Island, north-east Antarctic Peninsula: origin, geomorphology and physical and chemical limnology. Antarctic Science 25, 358–372.
Nývlt, D., Kopačková, V., Láska, K., Engel, Z., 2010. Recent changes detected on two glaciers at the northern part of James Ross Island, Antarctica. Geophysical Research Abstracts 12, EGU2010–EGU8102.
Nývlt, D., Košler, J., Mlčoch, B., Mixa, P., Lisá, L., Bubík, M., Hendriks, B.W.H., 2011. The Mendel Formation: evidence for Late Miocene climatic cyclicity at the northern tip of the Antarctic Peninsula. Palaeogeography, Palaeoclimatology, Palaeoecology 299, 363–384.
Phillips, W.M., Hall, A.M., Mottram, R., Fifield, L.K., Sugden, D.E., 2006. Cosmogenic ^{10}Be and ^{26}Al exposure ages of tors and erratics, Cairngorm Mountains, Scotland: timescales for the development of a classic landscape of selective linear glacial erosion. Geomorphology 73, 222–245.
Pudsey, C.J., Evans, J.E., 2001. First survey of Antarctic sub-ice shelf sediments reveals mid-Holocene ice shelf retreat. Geology 29, 787–790.
Pudsey, C.J., Murray, J.W., Appleby, P., Evans, J., 2006. Ice shelf history from petrographic and foraminiferal evidence, Northeast Antarctic Peninsula. Quaternary Science Reviews 25, 2357–2379.
Putkonen, J., Swanson, T., 2003. Accuracy of cosmogenic ages for moraines. Quaternary Research 59, 255–261.
Reimer, P.J., Baillie, M.G.L., Bard, E., Bayliss, A., Beck, J.W., Bertrand, C., Blackwell, P.G., Buck, C.E., Burr, G., Cutler, K.B., Damon, P.E., Edwards, R.L., Fairbanks, R.G., Friedrich, M., Guilderson, T.P., Hughen, K.A., Kromer, B., McCormac, F.G., Manning, S. Bronk, Ramsey, C., Reimer, R.W., Remmele, S., Southon, J.R., Stuiver, M., Talamo, S., Taylor, F.W., van der Plicht, J., Weyhenmeyer, C.E., 2009. Intcal09 and Marine09 radiocarbon age calibration curves 0–50,000 years Cal BP. Radiocarbon 51, 1111–1150.
Rinterknecht, V.R., Clark, P.U., Raisbeck, G.M., Yiou, F., Bitinas, A., Brook, E.J., Marks, L., Zelčs, V., Lunkka, J.-P., Pavlovskaya, I.E., Piotrowski, J.A., Raukas, A., 2006. The last deglaciation of the southeastern sector of the Scandinavian Ice Sheet. Science 311, 1449–1452.
Roberts, S.J., Hodgson, D.A., Sterken, M., Whitehouse, P.L., Verleyen, E., Vyverman, W., Sabbe, K., Balbo, A., Bentley, M.J., Moreton, S.G., 2011. Geological constraints on glacio-isostatic adjustment models of relative sea-level change during deglaciation of Prince Gustav Channel, Antarctic Peninsula. Quaternary Science Reviews 30, 3603–3617.
Rosenheim, B.E., Day, M.B., Domack, E., Schrum, H., Benthien, A., Hayes, J.M., 2008. Antarctic sediment chronology by programmed-temperature pyrolysis: Methodology and data treatment. Geochemistry Geophysics Geosystems 9, Q04005. http://dx.doi.org/10.1029/2007GC001816.
Simms, A.R., Lambeck, K., Purcell, A., Anderson, J.B., Rodriguez, A.B., 2007. Sea-level history of the Gulf of Mexico since the Last Glacial Maximum with implications for the melting history of the Laurentide Ice Sheet. Quaternary Science Reviews 26, 920–940.
Stenni, B., Masson-Delmotte, V., Johnsen, S., Jouzel, J., Longinelli, A., Monnin, E., Röthlisberger, R., Selmo, E., 2001. An oceanic cold reversal during the last deglaciation. Science 293, 2074–2077.
Sterken, M., Roberts, S.J., Hodgson, D.A., Vyverman, W., Balbo, A.L., Sabbe, K., Moreton, S.G., Verleyen, E., 2012. Holocene glacial and climate history of Prince Gustav Channel, northeastern Antarctic Peninsula. Quaternary Science Reviews 31, 93–111.
Stone, J.O., 2000. Air pressure and cosmogenic isotope production. Journal of Geophysical Research - Solid Earth 105, 23753–23759.
Stone, J.O., Balco, G.A., Sugden, D.E., Caffee, M.W., Sass III, L.C., Cowdery, S.G., Siddoway, C., 2003. Holocene Deglaciation of Marie Byrd Land, West Antarctica. Science 299, 99–102.
Storey, B.C., Fink, D., Hood, D., Joy, K., Shulmeister, J., Riger-Kusk, M., Stevens, M.I., 2010. Cosmogenic nuclide exposure age constraints on the glacial history of the Lake Wellman area, Darwin Mountains, Antarctica. Antarctic Science 22, 603–618.
Ward, G.K., Wilson, S.R., 1978. Procedures for comparing and combining radiocarbon age determinations: a critique. Archaeometry 20, 19–31.
Weaver, A.J., Saenko, O.A., Clark, P.U., Mitrovica, J.X., 2003. Meltwater Pulse 1A from Antarctica as a trigger of the Bølling-Allerød warm interval. Science 299, 1709–1713.
White, D.A., Fink, D., Gore, D.B., 2011. Cosmogenic nuclide evidence for enhanced sensitivity of an East Antarctic ice stream to change during the last deglaciation. Geology 39, 23–26.
Žák, J., Soejono, I., Janoušek, V., Venera, Z., 2012. Magnetic fabric and tectonic setting of the Early to Middle Jurassic felsic dykes at Pitt Point and Mount Reece, eastern Graham Land, Antarctica. Antarctic Science 24, 45–58.
Zale, R., Karlén, W., 1989. Lake sediment cores from the Antarctic Peninsula and surrounding islands. Geografiska Annaler 71 (A), 211–220.